J. Fluid Mech. (1980), *vol.* 99, *part* 1, *pp.* 1–11
Printed in Great Britain

Fluid flow in a hemispherical container induced by a distributed source of current and a superimposed uniform magnetic field

By R. E. CRAINE AND N. P. WEATHERILL
Faculty of Mathematical Studies, University of Southampton, England

(Received 15 March 1979 and in revised form 31 July 1979)

In arc welding electromagnetic forces are thought to be the major cause of motion in the weldpool, and it has recently been found by experimentalists that the application to the workpiece of a uniform magnetic field normal to the weldpool surface appears to stabilize the welding process. In this paper we investigate motion in a hemisphere due to a stationary distributed current source with a superimposed uniform magnetic field applied parallel to the axis of symmetry. When inertial effects are ignored and a simple source–sink model of the current source is introduced, we obtain an analytic solution for the fluid flow valid for low currents and low applied fields. A numerical scheme is then developed to solve the full nonlinear-flow problem and results are obtained for the source–sink model of the current source and for a more realistic numerically constructed distributed current source. For values of the externally applied magnetic field and the current flowing through the hemisphere typical of those occurring in practical welding situations we discover that the flow in an axial section through the pool is radially outwards on the free surface. This is in the opposite direction to that generally predicted by the theory when there is no superimposed magnetic field.

1. Introduction

Fusion welding is important in many industrial processes and in order to achieve consistently satisfactory welds much effort is being expended in attempts to ascertain the important mechanisms determining the shape of the weldpool.

The experiments of Woods & Milner (1971), Kublanov & Erokhin (1974) and Butsenieks *et al.* (1975, 1976) have shown the existence of vigorous motion in the weldpool, and it seems likely that this motion significantly influences the position of the solid–liquid boundary and hence the shape of the weldpool. These experiments also suggest that the motion is mainly caused by the electromagnetic $\mathbf{j} \times \mathbf{B}$ force, $\mathbf{j}$ being the current density induced in the material by the welding arc and $\mathbf{B}$ the corresponding magnetic induction.

In attempts to find the fluid flow in the weldpool theoreticians have modelled the current source in a number of ways. In most of the early work the welding arc was represented by a stationary point source of current on the surface of the material, but this model leads to the appearance of singularities in the velocity distribution. For further discussion of the point source representation the reader should consult Moffatt (1978) and Andrews & Craine (1978).

0022–1120/80/4456–8810 $02.00

In practice the current enters the material not at a point but over an area of the surface, and methods of modelling these distributed current sources have been put forward by a number of authors. Sozou (1972) considered the far-field solution in a semi-infinite fluid due to a disk source of current. Later Andrews & Craine (1976, 1978) proposed a current distribution arising from the combination of a point source and a ring sink and this gave a smooth velocity field in a hemispherical pool. The source-sink current distribution is fairly uniform over the surface of the pool, however, and one which more accurately models the concentrated current sources which occur in arc welding has recently been constructed numerically by Atthey (1978). Under normal welding conditions the linear solution of Andrews & Craine is restricted to small currents (only 1 or 2 A through the pool) whereas Atthey, also working with a hemispherical pool, solved the nonlinear flow problem numerically, using both the source–sink and numerically constructed current distributions, for currents through the pool of up to 100 A. A disk source of current of radius k on the surface of an oblate hemispheroidal pool of equatorial radius a (where $a > k$) has been considered in a recent paper by Sozou & Pickering (1978). They obtained an analytic solution when the inertial terms in the governing Navier–Stokes equations are neglected, the assumption previously made in Andrews & Craine (1976, 1978). Sozou & Pickering display solutions for various values of a/k, but under typical welding conditions their solutions are valid only for low currents.

Although the theoretical work outlined above has helped in the understanding of the complex mechanisms involved in arc welding, a problem which concerns experimentalists is the non-repeatability of results from experiments conducted under apparently identical conditions. Recently it has been found that the superposition of a uniform magnetic field over the weldpool and normal to the free surface produces more consistent results (Selyanenkov *et al.* 1975; Willgoss 1978). Any technique which stabilizes the welding process is potentially of great importance and research is now in progress to assess the practical implications of these observations.

In this paper we will consider in detail the fluid motion produced in a stationary hemispherical weldpool when a distributed source of current is applied to the plane face of the hemisphere, the free surface of the pool, and a uniform magnetic field, normal to the free surface, is superimposed over the pool. The basic equations are displayed in § 2 and two methods of representing a distributed current source are given in § 3. Neglecting the inertial terms in the Navier–Stokes equations and using the Andrews & Craine source–sink distribution of current we obtain in § 4 an analytic solution to the linear fluid flow problem which, under typical welding conditions, is valid for low applied currents (< 15 A). Although this analytic solution has limited validity it provides information on the qualitative features of the flow patterns and it proves a useful check on the accuracy of the numerical scheme developed in § 5. The stream-function-vorticity numerical method is used and a summary of the numerical results obtained is given in the following section. The results are discussed in § 7.

2. Basic equations

An electrically conducting incompressible fluid of density ρ and kinematic viscosity ν fills a hemispherical container of radius r_0. Spherical polar co-ordinates (r, θ, ϕ) are employed, the origin $r = 0$ being the centre of the plane face, which is a free surface,

and the axis $\theta = 0$ being the axis of symmetry into the fluid hemisphere. The current density $\mathbf{j}$ which is induced in the fluid by the applied current source gives rise to the magnetic induction $\mathbf{B}$, determined by Maxwell's equation

$$\nabla \times \mathbf{B} = \mu_0 \mathbf{j}, \tag{1}$$

where μ_0 is the permeability (m.k.s. units). Back E.M.F. effects are ignored (for further discussion see § 7).

If p and $\mathbf{v}$ denote the static pressure and velocity of the fluid respectively and we introduce the vorticity $\boldsymbol{\omega} = \nabla \times \mathbf{v}$, then the basic fluid flow equations to be solved are the momentum equation

$$\rho\left(\frac{\partial \mathbf{v}}{\partial t} + (\mathbf{v}.\nabla)\,\mathbf{v}\right) = -\nabla p + \mathbf{j} \times \mathbf{B} - \rho\nu\nabla \times \boldsymbol{\omega} \tag{2}$$

and the continuity of mass equation $\nabla . \mathbf{v} = 0$.

In this paper the resultant magnetic induction $\mathbf{B}$ is the sum of $\mathbf{B}_s$, a term arising directly from the current density induced by the applied source, and $\mathbf{B}_0$, the externally applied uniform magnetic field. We assume $\mathbf{B}_0$ is parallel to $\theta = 0$ and acts into the hemisphere and therefore, with respect to the spherical polar co-ordinate system, it is given by

$$\mathbf{B}_0 = B_0(\mu, -(1-\mu^2)^{\frac{1}{2}}, 0), \tag{3}$$

where $\mu = \cos\theta$. It is clear from equation (1) and the uniformity of $\mathbf{B}_0$ that the resultant value of $\mathbf{j}$ arises solely from the applied current source, which we assume is axisymmetric. It is convenient to introduce a (Stokes) stream function ψ and write

$$\mathbf{v} = \left(-\frac{1}{r^2}\frac{\partial \psi}{\partial \mu}, -\frac{1}{r(1-\mu^2)^{\frac{1}{2}}}\frac{\partial \psi}{\partial r}, w\right), \tag{4}$$

where both ψ and w are independent of ϕ. The continuity of mass equation is then identically satisfied.

The boundary conditions for the problem under discussion are

$$\psi = \frac{\partial^2 \psi}{\partial \mu^2} = \frac{\partial w}{\partial \mu} = 0 \quad \text{on} \quad \mu = 0, \tag{5}$$

$$\psi = \frac{\partial \psi}{\partial r} = w = 0 \quad \text{on} \quad r = r_0, \tag{6}$$

$$\psi = 0 \quad \text{on} \quad \mu = 1, \tag{7}$$

$$\mathbf{v} \text{ is finite throughout the hemisphere (particularly on } \mu = 1 \text{ and as } r \to 0). \tag{8}$$

The conditions on ψ are identical to those introduced in Andrews & Craine (1978) whilst equations (5c) and (6c) ensure that the shear stress and azimuthal velocity are zero on the free surface and solid–liquid interface respectively. The validity of assuming that the free surface is flat will be discussed in § 7.

3. Current distributions

Two distinct forms for the current density $\mathbf{j}$ will be used in later sections. Firstly following Andrews & Craine (1978) $\mathbf{j}$ is constructed from a point source a distance a above the free surface $\mu = 0$ and a point sink a distance b below this surface, with the

source and sink lying on the axis of symmetry and the total discharge of current being I. For this source–sink model the current density $\mathbf{j}$ has the form $(j_r, j_\theta, 0)$ whilst the corresponding induced field $\mathbf{B}_s$ is given by $\mathbf{B}_s = (0, 0, B_\phi)$. Series representations for j_r, j_θ and B_ϕ, when $r_0 < a$ and $r_0 < b$, may be found in Andrews & Craine 1978, equations (7) and (8).

Although the above current distribution enables an analytic solution to be found there is little variation in the normal component of $\mathbf{j}$, j_θ, on the free surface $\mu = 0$ of the pool and when $a = b = 2r_0$ around 90% of the total current I misses the pool. The obvious way of circumventing this problem by choosing $a \ll r_0$ leads to analytic difficulties and therefore in order to represent a realistic current source Atthey (1978) has constructed a numerical distribution by considering the current flowing in a plate of finite thickness g. Employing cylindrical co-ordinates (l, z) Atthey solves Laplace's equation for the electrostatic potential V subject to the boundary conditions,

$$\frac{\partial V}{\partial z} = j_0(l) \text{ on } z = 0, \quad \frac{\partial V}{\partial z} = 0 \text{ on } z = g, \quad \frac{\partial V}{\partial l} = 0 \text{ on } l = 0, \quad V = 0 \text{ on } l = L_0. \tag{9}$$

Conditions $(9a)$ and $(9b)$ imply that a normal flow of current $j_0(l)$ is prescribed on $z = 0$, the top surface of the plate, whereas there is no current flow across $z = g$, the bottom surface. Equation $(9c)$ follows from symmetry whereas $(9d)$ represents the assumption that at some radius L_0 (typically $3g$) the current flow has no z component. In later work we use, following Atthey (1978), the current distribution determined by

$$j_0(l) = \frac{Ie^{-(l/l_0)^2}}{\pi l_0^2(1 - e^{-(r_0/l_0)^2})}, \tag{10}$$

where we assume $r_0 = 2 \times 10^{-3}$ m, $l = 0{\cdot}4r_0$ and $g = 2r_0$. Since $l_0 \ll r_0 < g$ most of the current I flows through the hemispherical pool and this pool lies within the plate. The numerical current distribution introduced here is much more concentrated near the origin than the source–sink one and consequently it leads to greater currents in directions perpendicular to $\theta = 0$ than the corresponding source–sink models. Having determined V using (9) and (10) the current density follows directly from Ohm's law which, in the absence of back E.M.F.'s, is

$$\mathbf{j} = -\sigma \nabla V, \tag{11}$$

where σ is the electrical conductivity. The magnetic induction is then calculated using equation (1).

4. A linearized solution

4.1. *Analysis*

The system comprising the fluid-flow equation (2) and the boundary conditions (5) to (8) is extremely complex and, in general, only numerical solutions are possible. However, we show below that an analytic solution can be found when the source–sink current distribution is used and the left-hand side of equation (2) is neglected.

Omitting these terms in (2) and taking the curl of the resulting linear equation to eliminate the pressure we obtain

$$D\Gamma = -\sum_{n=1}^{\infty} d_n R^n (1 - \mu^2) P'_{n-1}(\mu) + A \tag{12}$$

and

$$D^2\Psi = -\sum_{n=1}^{\infty} R^{n+1}F_n(\mu), \tag{13}$$

where A is a constant, $P_n(\mu)$ is the Legendre polynomial of first degree and order n,

$$P_n'(\mu) \equiv \frac{dP_n}{d\mu}, \quad d_n = \left(\frac{r_0}{b}\right)^{n+1} + \left(-\frac{r_0}{a}\right)^{n+1}, \quad R = r/r_0, \quad D \equiv \frac{\partial^2}{\partial R^2} + \frac{1-\mu^2}{R^2}\frac{\partial^2}{\partial \mu^2} \tag{14}$$

and

$$\overline{w} = w\Big/\left(\frac{IB_0}{4\pi\rho\nu}\right), \quad \Gamma = R(1-\mu^2)^{\frac{1}{2}}\overline{w}, \quad \Psi = \psi\Big/\left(\frac{\mu_0 I^2 r_0}{8\pi^2\rho\nu}\right). \tag{15}$$

In deriving equations (12) and (13) we have used equation (3) and the series representations for $\mathbf{j}$ and $\mathbf{B}_s$ mentioned at the beginning of § 3. The solution of (13) subject to the conditions on Ψ in the set of boundary conditions (5) to (8) is precisely that found by Andrews & Craine (1978) and requires no further discussion.

The boundary condition (5) suggests that we seek a solution for w, and hence Γ, which is even in μ. In view of the form of the operator D it is therefore appropriate to express the right-hand side of equation (12), which contains Legendre polynomials of both odd and even orders, as an even function of μ. We therefore write

$$(1-\mu^2)P_{n-1}'(\mu) = \sum_{m=0}^{\infty}(1-\mu^2)\,a_{2m+1}^{(n)}\,P_{2m+1}'(\mu) \quad \text{for} \quad 0 \leqslant \mu \leqslant 1, \tag{16}$$

and deduce that (MacRobert 1947)

$$a_{2m+1}^{(n)} = \frac{(4m+3)\,n(n-1)}{(2m+1)\,(2m+2)}\int_0^1 P_{2m+1}(\mu)\,P_{n-1}(\mu)\,d\mu, \tag{17}$$

where use has been made of the fact that the $P_{2m+1}'(\mu)$ form an orthogonal set of functions with respect to the weighting factor $(1-\mu^2)$.

Using the relation (16) the solution of (12) which satisfies the conditions (5c) and (8) is

$$\Gamma = (1-\mu^2)\sum_{n=1}^{\infty}\left\{\beta_{2n-1}R^{2n}P_{2n-1}'(\mu) - d_n R^{n+2}\sum_{m=0}^{\infty}A_{2m+1}^{(n)}P_{2m+1}'(\mu)\right\}, \tag{18}$$

where

$$A_{2m+1}^{(n)} = d_n\,a_{2m+1}^{(n)}/\{(n+1)\,(n+2) - (2m+1)\,(2m+2)\}. \tag{19}$$

Note both the numerator and denominator on the right-hand side of equation (19) are zero when $n = 2m$, but in this special case a series expansion of the form (16) is unnecessary and we define $A_{2m+1}^{(2m)} = 0$. The remaining boundary condition (6c) determines β_{2n-1} and hence the non-dimensional azimuthal velocity $\overline{w}$ is given by

$$\overline{w} = \sum_{n=1}^{\infty}\sum_{m=0}^{\infty}A_{2+m1}^{(n)}\,(R^{2m+1} - R^{n+1})\,(1-\mu^2)^{\frac{1}{2}}\,P_{2m+1}'(\mu). \tag{20}$$

Table 1 lists the coefficients $A_{2m+1}^{(n)}$ for particular current distributions of interest.

The resultant flow of fluid in the hemispherical pool is a superposition of the azimuthal motion represented by (20) and the poloidal motion which follows from the stream function Ψ given by Andrews & Craine 1978, equation (23).

	$b/a = 1$					$b/a = 5$				
m	$n=1$	$n=2$	$n=3$	$n=4$	$n=5$	$n=1$	$n=2$	$n=3$	$n=4$	$n=5$
0	0	0	7·81	0	−0·48	0	−12·39	3·91	0	−0·24
1	0	0	6·84	0	0·85	0	0	3·42	−1·73	0·43
2	0	0	1·07	0	1·34	0	0	0·54	0	0·63
3	0	0	−0·12	0	0·27	0	0	−0·06	0	0·14
4	0	0	0·03	0	−0·04	0	0	0·02	0	−0·02
5	0	0	−0·004	0	0·0015	0	0	0·0001	0	0·005

TABLE 1. Coefficients $10^3 A^{(n)}_{2m+1}$ for two current distributions.

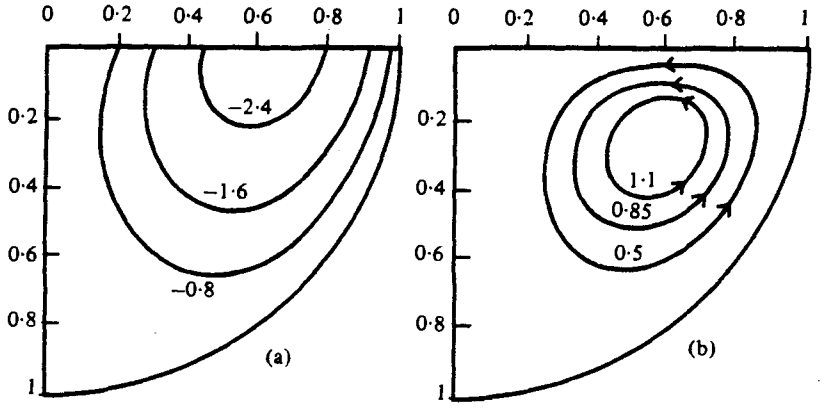

FIGURE 1. Flow patterns for analytic solution using source–sink current distribution with $b/a = 5$. Profiles of (*a*) $\overline{w} \times 10^3$ and (*b*) $\Psi \times 10^6$.

4.2. *Results*

Numerical results for the solutions $\overline{w}$ and Ψ discussed above are now presented. Since $\overline{w}$ is independent of ϕ it is displayed by showing lines of constant $\overline{w}$ on any axial section. The profiles of $\overline{w}$ and Ψ when $r_0/a = 0{\cdot}5$ and $b = 5a$ are shown in figure 1, the arrows on figure 1 (*b*) indicating the direction of flow. Observe from figure 1 (*a*) that the maximum azimuthal velocity occurs on the free surface. The expressions for $\overline{w}$ and Ψ have also been evaluated for a number of values of b/a, all greater than 1, and some profiles for Ψ may be found in Andrews & Craine (1978). The corresponding profiles for $\overline{w}$ are not given here since they exhibit the same qualitative features as figure 1 (*a*) except that the azimuthal velocity can have its maximum value in the bulk of the fluid.

The analytic solution is valid only for values of the applied current and applied magnetic field less than certain critical values. Inserting values of the parameters appropriate for the welding of steel, i.e. $\rho = 8 \times 10^3$, $\nu = 10^{-6}$, $r_0 = 2 \times 10^{-3}$ (m.k.s. units), careful investigation of the inertial terms reveals that their neglect is justified provided the applied current I is not more than 15 A and the applied magnetic field B_0 satisfies $IB_0 < 1{\cdot}5 \times 10^{-4}$. To model real welding situations, however, solutions for much larger I are required and these solutions can only be obtained using numerical schemes such as the one outlined below.

5. Numerical solution of the nonlinear problem

In this section we present a numerical solution of the time-dependent Navier–Stokes equations using the stream-function-vorticity approach. Although it seems an unnecessary complication to determine the solution of a steady-state elliptic problem by considering the time-dependent parabolic one, the solution of the latter from prescribed initial conditions using a step-by-step method is equivalent to the solution of the steady-state elliptic problem by an iterative technique. Discussions of the method used here, and other related ones, may be found in the survey articles of Roache (1972) and Orszag & Israeli (1974).

Let us denote the spherical polar components of $\mathbf{v}$ and $\boldsymbol{\omega}$ $(=\nabla\times\mathbf{v})$ by (u, v, w) and (ξ, η, ζ) respectively, and their non-dimensional counterparts by $(\bar{u}, \bar{v}, \bar{w})$ and $(\bar{\xi}, \bar{\eta}, \bar{\zeta})$. Introducing

$$u_0 = \mu_0 I^2/8\pi^2\rho\nu r_0, \quad \xi_0 = IB_0/4\pi\rho\nu r_0, \tag{21}$$

we define

$$\bar{u} = u/u_0, \quad \bar{v} = v/u_0, \quad \bar{\xi} = \xi/\xi_0, \quad \bar{\eta} = \eta/\xi_0, \quad \bar{\zeta} = r_0\zeta/u_0, \tag{22}$$

and observe that the definitions (15*a*, *c*) of $\overline{w}$ and Ψ are equivalent to $\overline{w} = w/r_0\xi_0$ and $\Psi = \psi/r_0^2 u_0$. Taking $s = \sin\theta$ it follows, with the use of equation (4), that

$$\bar{\xi} = \frac{1}{Rs}\frac{\partial}{\partial\theta}(s\overline{w}), \quad \bar{\eta} = -\frac{1}{R}\frac{\partial}{\partial R}(R\overline{w}), \quad \bar{\zeta} = \frac{1}{Rs}\left(-\frac{\partial^2\Psi}{\partial R^2} - \frac{1}{R^2}\frac{\partial^2\Psi}{\partial\theta^2} + \frac{\cot\theta}{R^2}\frac{\partial\Psi}{\partial\theta}\right). \tag{23}$$

The azimuthal component of equation (2) can be written in the non-dimensional form

$$\frac{\partial\overline{w}}{\partial\tau} + \frac{K^I}{4Rs}\operatorname{div}(Rs\overline{w}\bar{v}) = \frac{1}{Rs}\{\operatorname{div}\operatorname{grad}(Rs\overline{w}) - 2\operatorname{div}(\overline{w}\hat{\boldsymbol{\omega}})\} + \left\{\frac{4\pi r_0^2}{IB_0}\mathbf{j}\times\mathbf{B}\,.\,\hat{\boldsymbol{\phi}}\right\}, \tag{24}$$

where div and grad denote the divergence and gradient taken with respect to the co-ordinates (R, θ, ϕ) and the quantities $\hat{\boldsymbol{\omega}}$, τ and K^I are defined by

$$\hat{\boldsymbol{\omega}} = (s, \mu, 0), \quad \tau = \nu t/r_0^2, \quad K^I = \mu_0 I^2/2\pi^2\nu^2\rho. \tag{25}$$

Taking the curl of equation (2), the ϕ component of the resulting equation becomes

$$\begin{aligned}\frac{\partial\bar{\zeta}}{\partial\tau} = {} & K^B\left\{\frac{1}{R}\left(\frac{\partial}{\partial R}(R\bar{\xi}\overline{w}) + \frac{\partial}{\partial\theta}(\overline{\eta w})\right)\right\} - \frac{K^I}{4}\left\{\frac{1}{R}\left(\frac{\partial}{\partial R}(R\bar{\zeta}\bar{u}) + \frac{\partial}{\partial\theta}(\bar{\zeta}\bar{v})\right)\right\} \\ & + \frac{1}{R}\left\{\frac{1}{R}\frac{\partial}{\partial\theta}\left(\frac{1}{s}\frac{\partial}{\partial\theta}(s\bar{\zeta})\right) + \frac{\partial^2}{\partial R^2}(R\bar{\zeta})\right\} + \left\{\frac{8\pi^2 r_0^4}{\mu_0 I^2}\operatorname{curl}(\mathbf{j}\times\mathbf{B})\,.\,\hat{\boldsymbol{\phi}}\right\},\end{aligned} \tag{26}$$

where

$$K^B = B_0^2 r_0^2/2\nu^2\rho\mu_0.$$

In addition to the boundary conditions (5) to (8) we must satisfy

$$\bar{\zeta} = 0 \quad \text{on} \quad \mu = 0, \quad \bar{\zeta} = 0 \quad \text{on} \quad \mu = 1, \quad \bar{\zeta} = -\frac{1}{Rs}\frac{\partial^2\Psi}{\partial R^2} \quad \text{on} \quad R = 1, \tag{27}$$

$$\overline{w} = 0 \quad \text{on} \quad \mu = 1. \tag{28}$$

Conditions (27) follow directly from applying (5*a*, *b*), (6*a*) and (7) to equation (23*c*), whereas condition (28) is obtained from considerations of the forcing term and symmetry. To complete the specification of the problem we assume that the initial conditions are $\Psi = \bar{\zeta} = \overline{w} = 0$ at $\tau = 0$.

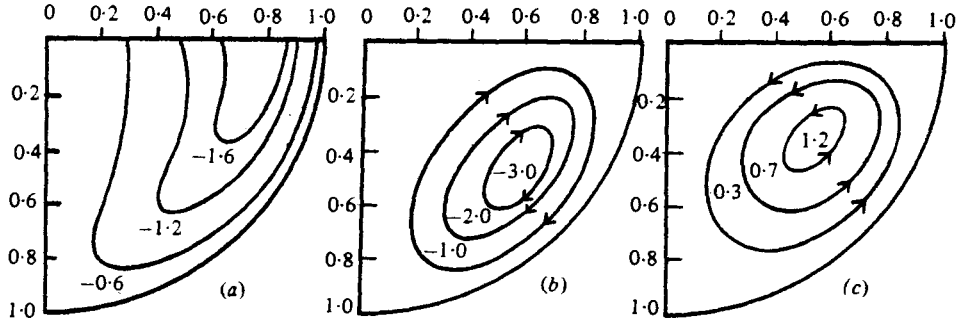

FIGURE 2. Flow patterns using source–sink current distribution with $b/a = 5$. Profiles of (*a*) $\overline{w} \times 10^3$, (*b*) $\Psi \times 10^6$ and (*c*) $\Psi \times 10^6$ for $\mathbf{B}_0$ zero.

The numerical solution is obtained by solving the finite difference analogues of equations (23*c*), (24) and (26) subject to the boundary conditions (5) to (8), (27) and (28). The Dufort–Frankel leap-frog method (Dufort & Frankel 1953) is used in obtaining the finite-difference form of the viscous terms in equations (24) and (26) and $\overline{w}$ and $\overline{\zeta}$ at a particular time step are then calculated from the finite-difference analogues of these equations. The updated values of the non-dimensional stream function Ψ are determined from equation (23*c*) using the iterative technique of successive over-relaxation. In finding $\overline{w}$, $\overline{\zeta}$ and Ψ the computational time is decreased by introducing a staggered mesh system. The calculation of $\overline{w}$, $\overline{\zeta}$ and Ψ is repeated for successive time steps until the solutions converge. The numerical scheme is stable provided the time step satisfies the Courant–Friedrichs–Lewy conditions.

The details of the numerical scheme are given in Weatherill (1980) whilst related discussions may be found in Roache (1972), Weir (1976) and Atthey (1978).

6. Results using numerical method

Before using the numerical scheme outlined in § 5 to solve the full nonlinear problem the accuracy of the programme was tested for two special cases. Firstly, when both the applied current and applied magnetic field are small the numerical method should give identical results to the analytic solution derived in § 4. This correlation was confirmed for a variety of values of $b/a (\geqslant 1)$ and for a number of values of $K^I (< 1{\cdot}8 \times 10^3)$ and $K^B (< 2 \times 10^{-2})$. On a 15×15 mesh, for all cases considered, the numerical solution of section 5 differs from the analytic solution obtained in § 4.1 by a maximum of 1 %.

A second test is possible when the applied field B_0 is zero but $K^I > 1{\cdot}8 \times 10^3$. In this situation the numerical scheme gives results, on a 15×15 mesh, which agree with those obtained by Atthey (1978) to within 0·01 %.

With the above tests completed we now use our numerical scheme to obtain results for larger K^I and K^B. A 15×15 mesh was used for all the numerical solutions which we discuss. A number of results were obtained on a finer mesh but the solutions were extremely close to those found on the 15×15 mesh.

First we restrict attention to the source–sink model of the current source. Assuming $r_0/a = 0{\cdot}5$ and $b = 5a$, and choosing $K^I = 2 \times 10^6$ and $K^B = 5 \times 10^3$ (equivalent under normal welding conditions to an applied current of 500 A and an applied magnetic field of 5×10^{-3} T) the profiles of $\overline{w}$ and Ψ obtained from the numerical solution are shown in figures 2(*a*, *b*) respectively. With no applied magnetic field but the same

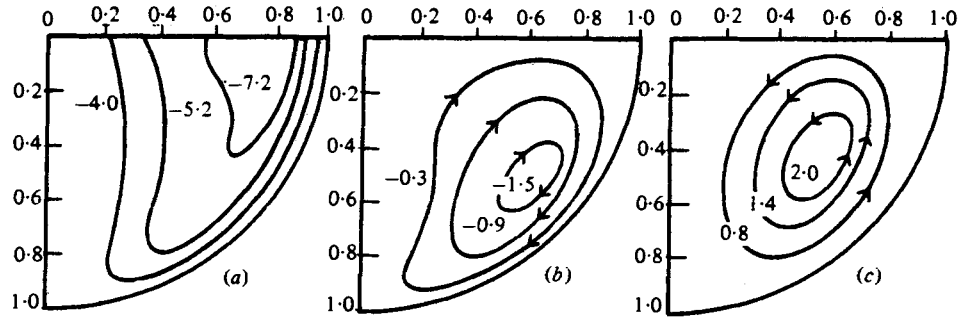

FIGURE 3. Flow patterns using numerically constructed distribution. Profiles of (*a*) $\overline{w} \times 10^2$, (*b*) $\Psi \times 10^3$ and (*c*) $\Psi \times 10^3$ for $\mathbf{B}_0$ zero.

applied current, K^I is unchanged, $K^B = 0$, the azimuthal velocity $\overline{w}$ is identically zero and the solutions for Ψ is shown in figure 2(*c*). Figure 2(*b*) reveals a poloidal flow in which the fluid flows radially outwards on the top surface, in contrast to the flow without an applied field displayed in figure (2*c*) where the flow is radially inwards on this surface. We observe from figure (2*a*) that $\overline{w}$ is a maximum on the upper surface. Results have also been obtained for different values of b/a. When $b/a = 1$ and a magnetic field is applied the figure for Ψ shows counter-rotating loops in the r, θ plane. As b/a increases from 1, the upper loop decreases in size until it disappears completely before b/a reaches the value 5. When $b/a > 5$ the flow patterns change little from those shown in figure 2.

Secondly, and perhaps more importantly, we consider the numerical results obtained when the applied current source is the realistic one proposed by Atthey (1978) and discussed in § 3. Using this numerical current distribution in the forcing terms in equations (24) and (26) and taking $K^I = 2 \times 10^4$ and $K^B = 5 \times 10^3$ (with typical welding parameters this is equivalent to assuming an applied current of 50 A and an applied magnetic field of $5 \times 10^{-3} T$) the results are displayed in figures 3(*a*, *b*). Figure 3(*c*) shows the results with zero applied field. Results obtained for different thicknesses of plate indicate similar flow patterns.

The most important feature of the above results is the reversal in the direction of flow of fluid in the r, θ plane, caused by application of the uniform magnetic field, and we now seek to explain this phenomenon.

When equation (3), the Navier-Stokes equation with an electromagnetic forcing term $\mathbf{j} \times \mathbf{B}$, is written in terms of spherical polar co-ordinates inspection of the resulting radial and angular (θ) equations reveals that the only non-zero terms involving the azimuthal velocity w represent a centrifugal force $w^2/r \sin\theta$ per unit mass acting in a direction perpendicular to the axis (radially outwards if cylindrical co-ordinates were adopted). In most situations of practical interest the numerical results show that w is much larger than both u and v, and therefore the motion in the r, θ plane is governed by the relative magnitudes of the centrifugal force and the r and θ components of the electromagnetic forcing term. A qualitative explanation for the flow patterns in figures 2(*b*) and 3(*b*) is now possible.

As first noted by Shercliff (1970) the current component normal to the axis $\mu = 0$ provides the forcing term which drives motion in the r, θ plane and in our problem it is the same current component which drives the azimuthal motion or swirl. For the

current distributions leading to figures 2 and 3 the component normal to the axis has its maximum value on the free surface and so it is not surprising that in these cases the non-dimensional $\overline{w}$, and hence w, achieves its maximum value on this surface. Consequently there is a large centrifugal force acting radially outwards along $\mu = 0$ and it is straightforward to show that the ratios of this force to the r and θ components of $\mathbf{j} \times \mathbf{B}$ are large in the situations leading to figures 2 and 3. The centrifugal force therefore overcomes the electromagnetic force, which is trying to move the fluid on the top surface radially inwards, and the resulting motion is radially outwards on $\mu = 0$.

With the velocity components determined the streamlines can be calculated by numerical integration of the usual equation. Without solving this equation it is easy to see that the streamlines will look similar to coiled springs, although their exact shape will depend on the relative magnitudes of u, v and w. It follows from (25c) and the definition of K^B that $(K^B/K^I)^{\frac{1}{2}}$ indicates the ratio of the applied magnetic field to the self-field and hence the ratio of the toroidal body force to the poloidal one. Taking the source–sink model with $b = 5a$, $r_0 = 2 \times 10^{-3}$ m, $I = 10$ A and $B_0 = 10^{-6}$ T we find that $(K^B/K^I)^{\frac{1}{2}} = 5 \times 10^{-4}$ and in this case u and v are much greater than w. However, in the situations leading to figures 2 and 3, which reflect typical welding conditions the quantity $(K^B/K^I)^{\frac{1}{2}}$ is 0·1 and 1 respectively and the value of w is much greater than that of either u or v.

7. Discussion

Most of the results presented in § 6 apply to normal welding conditions and it is therefore of vital importance to ascertain whether our results are confirmed by experimental evidence. Inserting values for the parameters appropriate to the welding of steel our numerical results predict maximum azimuthal velocities of between 10 and 20 cms^{-1}. The latter are of comparable magnitude to those obtained in the experiments of Willgoss (1978). Since the velocity components u and v are an order of magnitude less than w it is difficult to observe experimentally whether the fluid moves inwards or outwards on the free surface.

There is indirect experimental evidence, however, to support our flow patterns. With typical welding parameters we find that the Péclet numbers associated with our flows are of order 10 and so it is natural to expect that convection within the weldpool will significantly alter the position of the liquid–solid boundary. With an applied magnetic field the fluid flow under realistic welding conditions is radially outwards on the free surface (figure 3b) and therefore we anticipate that the width to depth ratio of the weldpool is greater than two. Experiments conducted by Willgoss (1978) confirm that this is the case.

An important restriction on the validity of our solutions concerns the free surface. In all the results derived earlier this surface has been assumed flat although in general this assumption is not valid. In the linear flow régime the analytic solution derived in § 4.1 can be used to determine the surface's approximate deformation (see Sozou & Pickering 1976, 1978). Slightly modifying their method and inserting appropriate values for the parameters it is found that the maximum deformation is extremely small compared with the depth of the pool. For further details the reader should consult Weatherill (1980).

A detailed calculation of the depression for the full nonlinear problem, which must be accomplished by a numerical routine, is a major task (see Roache 1972, p. 180) and any values so obtained would only be approximate since the fluid flow changes instantaneously with the free surface. Finding the exact shape of this surface is therefore an extremely complicated coupled problem. However, an order of magnitude analysis (based on the method of Sozou & Pickering 1976, 1978) is possible and Weatherill (1980) has shown that, under conditions appropriate to figures 2 and 3, the free surface may be distorted by an amount which is approximately 10 % of the radius of the pool.

Another crucial assumption in our analysis is the neglect of back E.M.F. effects. It is not difficult to deduce that the maximum value of the Hartmann number M which is defined by $M = 2K^B\mu_0\nu\sigma$, the electrical conductivity σ being typically 8×10^5 in a weldpool, for the situations appropriate to figures 1 to 3 is 0·05 and hence the neglect of the $\sigma\mathbf{v} \times \mathbf{B}$ term in equation (11) is justified. Moreover, a careful investigation of the magnitudes of the relevant terms reveals that the azimuthal eddy currents generated when the poloidal motion crosses the applied magnetic field lines do not result in a forcing term which significantly affects the poloidal motion.

The authors are indebted to the referees for some helpful comments, to Dr D. R. Atthey and Dr R. A. Willgoss for making available copies of their papers prior to publication and NPW is grateful to the Science Research Council and Marchwood Engineering Laboratories, CEGB for the award of a CASE studentship.

REFERENCES

ANDREWS, J. G. & CRAINE, R. E. 1976 *C.E.G.B. Lab. Note* R/M/N919.

ANDREWS, J. G. & CRAINE, R. E. 1978 *J. Fluid Mech.* **84**, 281.

ATTHEY, D. R. 1978 *C.E.G.B. Lab. Note* R/M/N1018.

BUTSENIEKS, I. E., KOMPAN, YA. YU., SHARAMKIN, V. I., SHILOVA, E. I. & SHCHERBININ, E. V. 1975 *Magnetohydrodyn.* **11**, 395 (transl. in English).

BUTSENIEKS, I. E., PETERSON, D. E., SHARAMKIN, V. I. & SHCHERBININ, E. V. 1976 *Magnetohydrodyn.* **12**, 70 (transl. in English).

DUFORT, E. C. & FRANKEL, S. P. 1953 *Maths. Comput.* **7**, 135.

KUBLANOV, V. & EROKHIN, A. 1974 *Int. Inst. Weld. Doc.* no. 212-318-74.

MACROBERT, T. M. 1947 *Spherical Harmonics*, p. 92. Methuen.

MOFFATT, H. K. 1978 *Z. angew. Math. Mech.* **58**, T65.

ORSZAG, S. A. & ISRAELI, M. 1974 *Ann. Rev. Fluid Mech.* **6**, 281.

ROACHE, P. J. 1972 *Computational Fluid Dynamics*. Albuquerque: Hermosa.

SELYANENKOV, V. N., BLINKOV, V. A., KAZAKOV, I. V. & BASCHENKOV, V. E. 1975 *Welding Prod.* **11**, 5 (transl. in English).

SHERCLIFF, J. A. 1970 *J. Fluid Mech.* **40**, 241.

SOZOU, C. 1972 *Phys. Fluids* **15**, 272.

SOZOU, C. & PICKERING, W. M. 1976 *J. Fluid Mech.* **73**, 641.

SOZOU, C. & PICKERING, W. M. 1978 *Proc. Roy. Soc.* A **362**, 509.

WEATHERILL, N. P. 1980 Magnetohydrodynamic flow in a weldpool. Ph.D. thesis. University of Southampton.

WEIR, A. D. 1976 *J. Fluid Mech.* **75**, 49.

WILLGOSS, R. A. 1978 *C.E.G.B. Rep.* R/M/R269.

WOODS, R. A. & MILNER, D. R. 1971 *Weld. J. Res. Suppl.* **50**, S163.